

# Nanobainite Generated in Low- and Medium-Carbon Steels via an Economical Alloying Strategy

Mohamad Akram,\* Heinz Palkowski, and Mohamed Soliman

A low-cost strategy for generating fast transforming nanobainitic (nB) steels in low- and medium-carbon alloys is investigated. Accelerating the bainite transformation relies on adding 0.7–3 wt% Al. Alloys and heat treatments are designed via thermodynamic calculations and dilatometry. nB microstructures are generated via isothermal holding and continuous cooling. The microstructures generated are investigated via microscopy and mechanical characterization. Incubation periods less than 150 s as well as isothermal transformation times ranging from 2000 to 4000 s are recorded for all conditions. Increasing the Al content from 0.7 to 2.8 wt% lowers the incubation and transformation times from 150 to 15 s and 3000 to 2000 s, respectively, at a cost of a reduction in tensile strength and elongation % (EL%) from 1330 to 1270 MPa and from 13.5 to 7.7%, respectively. The introduction of  $\delta$ -ferrite to the microstructure of the high Al alloy increased EL% up to 16% and reduced the tensile strength to 1105 MPa. Continuous cooling at a rate of  $0.03 \text{ K s}^{-1}$  increased the tensile strength by 100 MPa at similar EL%. Lowering the cooling rate to  $0.003 \text{ K s}^{-1}$  yielded similar properties as isothermal treatment because most of the transformation is concluded near the starting temperature.

## 1. Introduction

The extension of the carbide-free nanobainitic (nB) steel concept into medium- and low-carbon (LC) steels is of considerable interest to both the industry and researchers in this field. High-carbon (C) percentages in the range of 0.6–1 wt% required for the generation of the nB microstructure endow these alloys with poor weldability owing to the generation of brittle martensite in the

heat affected zone. In addition to that, the high strength of these steels coupled with their resistance to tempering hinders their formability.<sup>[1,2]</sup> Earlier studies report the difficulty of nB generation in LC steel, contrary to the effect of C, suppressing the martensite start temperature ( $M_s$ ) via substitutional alloying reduces the difference between the bainite start ( $B_s$ ) and  $M_s$  temperatures.<sup>[1]</sup> However, more recent attempts have been successful in obtaining nB microstructures at increasingly lower C contents.

Garcia-Mateo et al. reported several paths to generating nB from LC steels, with the basic idea being the generation of a phase from which C is to partition into austenite, stabilizing it, and enabling bainitic transformation below the regular  $M_s$  of the alloy.<sup>[3,4]</sup> Quenching and partitioning, austempering below  $M_s$ , and two-step austempering are among some of the approaches mentioned. In addition to that, reducing the prior austenite grain size,


whether by alloying or austempering, serves to lower the  $M_s$ , facilitating the low-temperature austempering of steels with lower C contents.<sup>[3]</sup>

Foughani et al.<sup>[5]</sup> reported generating nB microstructure in a 0.48 wt% C high Si steel alloy via a two-step isothermal process at 290 and 250 °C. The resulting structure recorded tensile strengths above 1.5 GPa at elongations to rupture (EL%) in excess of 12% and maximum transformation times of 12 h.<sup>[5]</sup> The lowest C content recorded for a nB alloy was reported as 0.26 wt% by Soliman et al.<sup>[6]</sup> produced via a two-step austempering process.<sup>[6]</sup> This was further confirmed via experiments on another alloy with a C content of 0.26 wt% by Mousalou et al.<sup>[7]</sup>

Another promising concept that has not been thoroughly covered in the literature is that of continuous cooling. The continuous partitioning of C into austenite, stabilizing it as the temperature drops, would ensure the continuous decrease in  $M_s$ , along with the generation of finer bainitic ferrite structures not attainable via isothermal or two-stage austempering. Soliman et al.<sup>[6]</sup> continuously cooled an 0.26 wt% C alloy from  $M_s + 20 \text{ K}$  at two different cooling rates; however, martensite was formed in both cases.<sup>[6]</sup> Indeed, the first successful production of martensite-free nB produced by continuous cooling was reported by Das and Haldar<sup>[2]</sup> in a 0.34 wt% C, high Si steel alloy at a rate of  $1 \text{ K min}^{-1}$ , simulating the cooling rate they measured during strip coiling. Heat-treated samples via either dilatometry or salt bath + oven recorded tensile strengths of around 1400 MPa with

M. Akram, H. Palkowski, M. Soliman  
Institute of Metallurgy  
Clausthal University of Technology  
38678 Clausthal-Zellerfeld, Germany  
E-mail: mohamad.abdelaziz@tu-clausthal.de

M. Soliman  
Faculty of Engineering  
Galala University  
Galala City 43511, Egypt

 The ORCID identification number(s) for the author(s) of this article can be found under <https://doi.org/10.1002/srin.202100575>.

© 2021 The Authors. Steel Research International published by Wiley-VCH GmbH. This is an open access article under the terms of the Creative Commons Attribution-NonCommercial License, which permits use, distribution and reproduction in any medium, provided the original work is properly cited and is not used for commercial purposes.

DOI: 10.1002/srin.202100575

**Table 1.** Chemical composition of the studied alloys in wt%.

Alloy	C [wt%]	Mn [wt%]	Si [wt%]	Al [wt%]	Mo [wt%]	Fe [wt%]
B1	0.32	2.78	1.82	0.73	0.24	Bal.
B2	0.30	2.95	0.55	2.1	0.23	Bal.
B3	0.31	2.74	0.31	2.8	0.24	Bal.
B4	0.23	4.17	0.31	3.0	0.24	Bal.

22% EL.<sup>[2]</sup> A more recent follow-up study investigated the promising wear properties of the aforementioned alloy which improved during wear testing owing to the retained austenite grains transforming under load to martensite.<sup>[8]</sup> More recent attempts to design nB alloys for continuous cooling were undertaken by Hasan et al. who reported bainitic microstructures with lamellar thicknesses of 120–300 nm.<sup>[9]</sup>

The aim of this study is the generation of a fast transforming, medium and LC nB steel alloys as better formability and weldability alternatives to the commonly reported high-carbon nB steels. Another major aim for this investigation is bypassing the martensite formation during continuous cooling problem encountered via accelerating the bainitic transformation.<sup>[6]</sup> This is to be achieved in an economically feasible manner by the addition of Al instead of the commonly used, more expensive Co.<sup>[10,11]</sup> A further advantage of increasing Al content is that lower amounts of Si, an element that causes deterioration in the surface quality of hot-rolled products when added in large amounts, are required.<sup>[10,12]</sup>

## 2. Experimental Section

The alloys studied were cast in a vacuum furnace with dimensions 165 × 145 × 60 mm<sup>3</sup>, homogenized for 48 h, followed by cooling for 12 h by switching off the oven. The homogenized blocks were hot-rolled at 1100 °C to 12 mm thickness using a 12" 2-high rolling machine followed by oven cooling. The homogenization, cooling hereafter and oven cooling after rolling took place under argon protection gas conditions. The compositions of the rolled plates are given in **Table 1**.

The alloying concept utilized in accelerating the bainitic transformation is a combination of LC steels coupled with an increase in Al content between 0.73 and 3.0 wt%. Both high Al and LC contents would lead to a low hardenability as well as a high martensite start temperature; hence, Mn amounts of 2.74–2.95 wt% were added to improve hardenability. Mo was added to counter temper embrittlement as well as to improve hardenability, and the amount of Si was reduced with the increase of Al because Al serves its role of suppressing carbide formation. The amount of Mn in alloy B4 was further increased to 4.17 wt% to compensate for its lower C content of 0.23 wt%. High Al contents in steel are reported to contract the  $\gamma$ -region in the phase diagram into what is known as the  $\gamma$ -loop.<sup>[13]</sup> As the Al content is increased,  $\gamma$ -loop is shifted toward higher C contents making full austenitization only possible for high C alloys, which is not ideal for the generation of nB. ThermoCalc was used in the alloy design phase to predict the min. C content required to avoid the  $\gamma$ -loop for the high Al B3 and B4 alloys which were found to be 0.22 and 0.17 wt%, respectively.

Thermodynamic simulations were performed using ThermoCalc software to estimate the austenitization temperatures of the alloys under investigation. Ø 5 mm × 10 mm cylindrical dilatometry specimens, ASTM E8 subsize round tensile specimens with a gauge length of 12.5 mm and gauge diameter of Ø 2.5 mm, and ASTM E23 subsize V-notched Charpy impact specimens with dimensions of 5 × 5 × 50 mm<sup>3</sup> were machined in rolling direction from the rolled steel plates. Dilatometric experiments were conducted on a Bähr DIL805A using quartz specimen holders for thermal cycles not exceeding 1100 °C and alumina ones for cycles above 1100 °C. Isothermal as well as continuous cooling treatments were performed according to the thermal cycles illustrated in **Figure 1a,b**, respectively. Subsize tensile and impact test specimens were chosen to enable their heat treatment in the dilatometer under controlled heating/cooling rates as well as under vacuum. Further details on the choice of austempering temperatures and cooling rates are discussed in the results section.

Metallographic specimens were ground and polished using standard techniques; a 3% nital solution was used for etching. The specimens were analyzed using an Olympus BX60M light

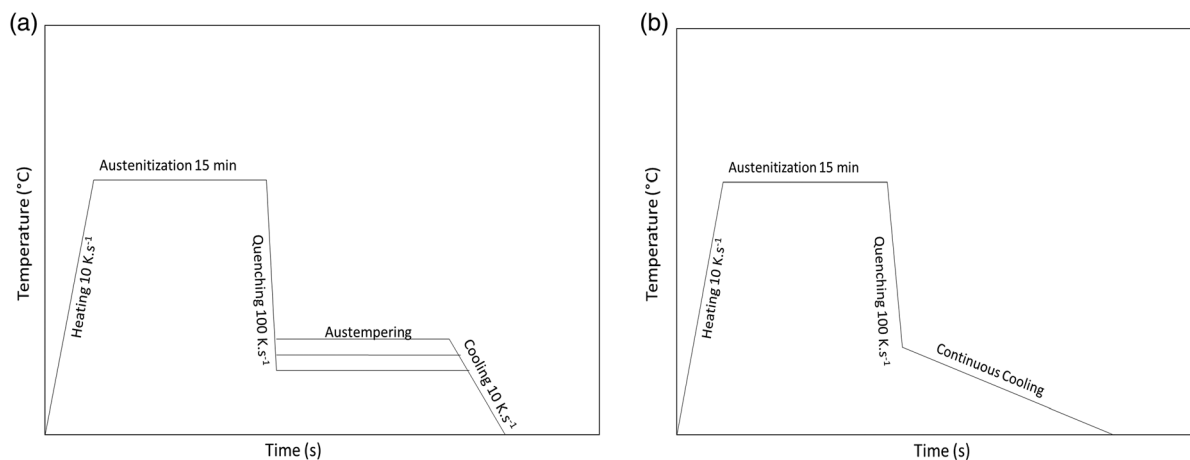


**Figure 1.** Heat treatment cycles utilized to generate the bainitic microstructures via a) isothermal transformation and b) continuous cooling.

optical microscope (LOM). The systematic manual point count method was used to determine the volume fraction of  $\delta$ -ferrite in the microstructure of the B4 alloy. Deep nital etching and gold sputtering were further employed for scanning electron microscope (SEM) analysis. The SEM images were used to measure the bainite thickness with the assistance of ImageJ image analysis software; a total of 100 measurements were taken per specimen. Quenched martensitic specimens were tempered at 550 °C for 48 h according to the procedure described in Soliman and Palkowski,<sup>[14]</sup> followed by metallographical preparation and etching using the Bechet–Beaujard reagent and then were analyzed under LOM to reveal the prior austenite grain size (PAGS)<sup>[15]</sup>; the grain size measurements were performed using the ImageJ software.

Vickers (HV30) hardness testing was performed according to ASTM E92-83 on transformed dilatometry specimens after grinding down to 400 grid size before testing via Wolpert hardness tester equipped with a digital measurement system. Tensile testing was performed on a Zwick/Roell universal testing machine with a 250 kN load cell. The machine is equipped with a video extensometer for accurate strain measurements.

Selected specimens transformed in dilatometer were sent for transmission electron microscopy (TEM) analysis to the Central Facility for Electron Microscopy (GFE) at RWTH Aachen to be investigated using a 200 kV Tecnai F20 TEM. The preparation of the specimens was performed by means of focused ion beam (FIB) technology using FEI STRATA FIB 205. Transformed dilatometry specimens were polished and analyzed using a Panalytical Empyrean DY1654 XRD diffractometer with a Cu  $K_{\alpha}$  radiation with 1.54 Å wavelength at 40 kV and 40 mA. Step scanning was performed in the range from 10° to 70° at a step value of 0.026° and 100 s of scanning time at each value of  $2\theta$ . Retained austenite ( $\gamma_r$ ) percentages were calculated from the integrated intensities of the (111), (200), (220), and (311) austenite diffraction peaks and the (110), (200), (211), (220) ferrite diffraction peaks according to the method described by Cullity and Stock.<sup>[16]</sup>

### 3. Results and Discussion

#### 3.1. Thermodynamic Simulation

Discrepancies were detected between the thermodynamically simulated results using ThermoCalc and the experimental findings. **Figure 2** indicates that alloys B1 to B4 are predicted to be fully austenitizable at the marked temperatures (Ae3). However, LOM results at different austenitizing temperatures imply the increasing inaccuracy of the TCFE9 database with increasing Al content. Temperatures of 950 and 1000 °C were insufficient to fully austenitize alloys B1 and B2, which only fully austenitized at 1050 °C. On the other hand, B3 required an even higher austenitization temperature of 1170 °C. While alloy B4 was originally designed to avoid the  $\gamma$ -loop and enable full austenitization, microscopic investigations after quenching from different austenitizing temperatures (**Figure 3**) imply that the alloy is located before the  $\gamma$ -loop. This is further supported by  $\delta$ -ferrite amount measurements, displayed in **Figure 4**, and shows that the amount of  $\delta$ -ferrite drops to a

minimum of around 12 vol% at 1200 °C before increasing again with increasing temperature. Similar discrepancies between ThermoCalc simulations and experimental findings were reported in the literature for high C, high Al nB steels.<sup>[17]</sup>

**Table 2** shows both the austenitization temperatures predicted by ThermoCalc and those chosen for experimental investigation, as well as the expected  $\delta$ -ferrite vol% corresponding to the chosen austenitization temperature. A  $\delta$ -ferrite amount of 12 vol% was allowed for B4 as it was not possible to obtain ferrite free microstructure in it. For this alloy the effect of  $\delta$ -ferrite on the kinetics and final properties of high Al nB alloys was analyzed.

The presence of 12%  $\delta$ -ferrite is expected to cause a deviation of the compositions of  $\delta$ -ferrite and parent austenite (and consequently bainitic ferrite and retained austenite) from the nominal composition of the alloy. ThermoCalc was used to calculate the composition of the austenite phase corresponding to a microstructure with 12% ferrite. The parent austenite in B4 was calculated to be marginally enriched with carbon at 0.24 wt% as well as manganese at 4.22 wt%; additionally, an insignificant drop in Al content, corresponding to a value of 2.98 wt%, was calculated for the parent austenite.

Specimens were heated at a rate of 10 K s<sup>-1</sup> to their respective austenitization temperature, followed by isothermally holding for 15 min. This was followed by quenching at a rate of 100 K s<sup>-1</sup> to an austempering temperature of 310 °C for B1 and 350 °C for B1 through B4, where the specimens were isothermally held until the completion of the bainite reaction. The methodology used to determine the transformation time is reported elsewhere in Akram et al.<sup>[17]</sup> The selection of the bainite transformation temperatures is based on the dilatometric measurements of  $M_s$ , which recorded 296, 318, 310, and 315 °C in alloys B1, B2, B3, and B4, respectively. For the continuous cooling investigations, a similar thermal cycle was utilized; however, specimens were quenched to 350 °C (and 310 °C for B1) after austenitization, followed by slow cooling at cooling rates of 0.3, 0.03, and 0.003 K s<sup>-1</sup> to determine the order of magnitude of the rate required for a successful conclusion of the transformation without martensite formation. The heat treatment cycles used for the austempering and continuous cooling experiments are provided in **Figure 1**. Owing to the different austenitization temperatures used for the alloys under investigation, the PAGS was measured and found to be 99  $\mu$ m for B1, 97  $\mu$ m for B2, further increasing to 122  $\mu$ m for B3 owing to its higher austenitization temperature, followed by a drop back to 89  $\mu$ m for B4. Similar observations of the PAGS increasing with austenitization temperature and then dropping back with the introduction of  $\delta$ -ferrite into the microstructure of nB alloys were reported for high C, high Al nB alloys in Akram et al.<sup>[17]</sup> Optical micrographs of the etched specimens for PAGS measurements are presented in **Figure 5**.

#### 3.2. Kinetics of Bainite Formation

**Figure 6a** shows the relative change in length versus time curves obtained from dilatometry under the isothermally transformed conditions. The incubation times for all the conditions studied are around 100 s, with the slowest value recorded for B1

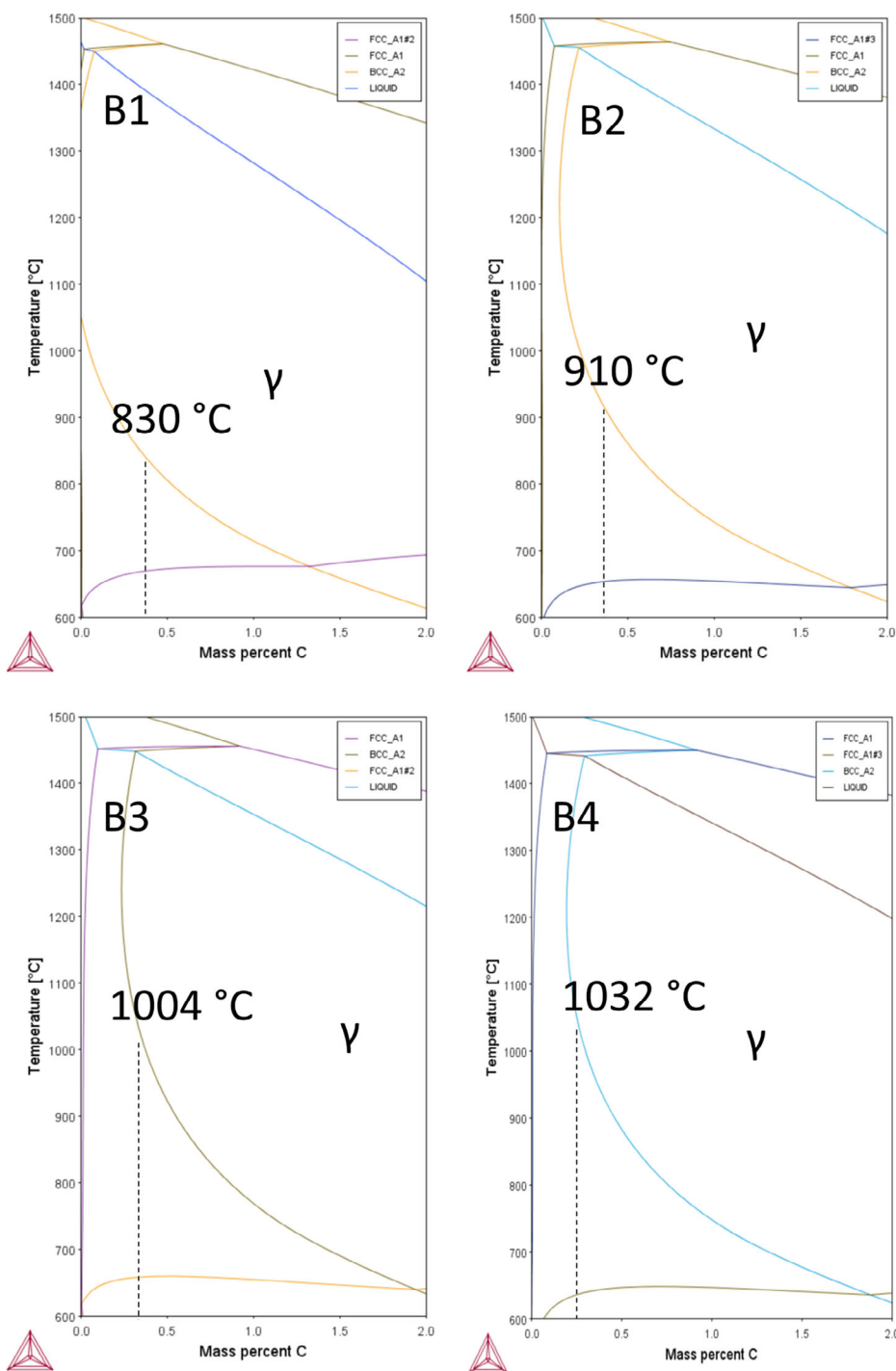


**Figure 2.** Phase diagrams of the alloys B1 through B4 simulated via ThermoCalc software.

transformed at 310 °C at 120 s, while the fastest value was recorded by B3 at 10 s. Transformation times for all the isothermal conditions tested (Figure 6a) are within the 2000–4000 s range, the highest of which is around what is usually reported in the literature for similar alloys.<sup>[6,7]</sup> Figure 6b illustrates the change in transformation time with the Al content. The fastest transformation time of 2000 s is recorded for the B3 alloy with

the highest Al content regardless of its higher PAGS. A finer PAGS is reported in the literature to accelerate the bainite formation kinetics,<sup>[18]</sup> Additionally, relying on Al to accelerate the transformation necessitates higher austenitization temperatures which translate to larger PAGS and in turn would slow the transformation kinetics. However, the present results indicate that an Al addition of 3 wt% is sufficient to counteract the

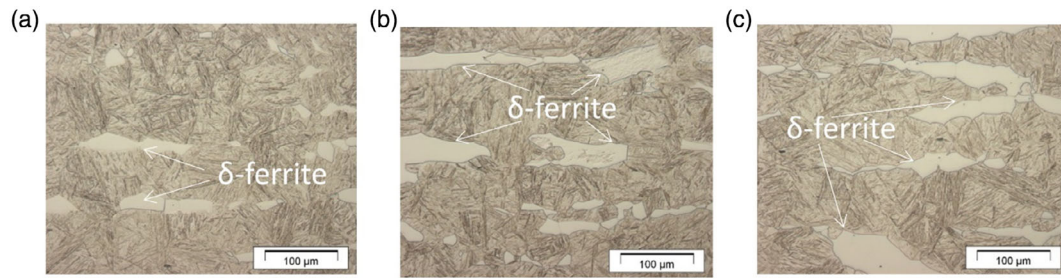


**Figure 3.** LOM images of alloy B4 austenitized for 15 min at a) 1200 °C, b) 1250 °C, and c) 1300 °C followed by quenching.

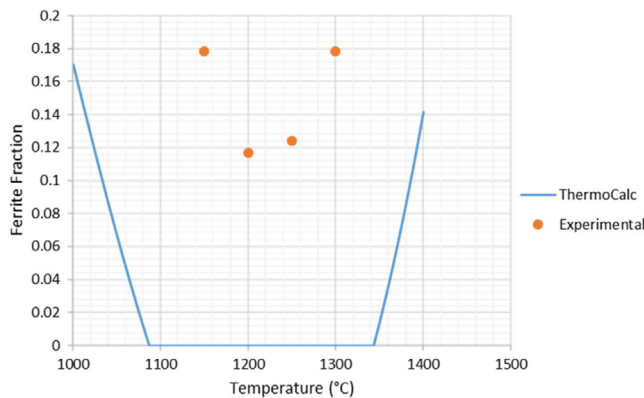


**Figure 4.** Experimental and ThermoCalc simulated values of the change of the  $\delta$ -ferrite fraction with the austenitization temperature.

**Table 2.** Theoretically predicted  $A_{e3}$  temperatures, applied austenitization, and austempering temperatures as well as the corresponding  $\delta$ -ferrite content for alloys B1–B4.

Alloy	Theoretical $A_{e3}$ temperature [°C]	Applied austenitization temperature [°C]	$\delta$ -Ferrite amount [vol%]	Austempering temperature [°C]
B1	830	1050	0	310, 350
B2	910	1050	0	350
B3	1004	1170	0	350
B4	1032	1200	12	350

retarding effect of larger PAGS and still yield a faster transformation. Conversely, the longest transformation times are recorded for alloy B1 transformed at 310 °C as well as B4 transformed at 350 °C. In the case of B1, it has the lowest Al content among all of the alloys studied, which coupled with the lower transformation temperature of 310 °C leads to slower transformation kinetics and a transformation time of 4000 s. On the other hand, the parent austenite in B4 possesses a high Al content of 2.98 wt%, a lower C content of 0.24 wt%, and 12 vol%  $\delta$ -ferrite in its microstructure which are factors expected to accelerate the transformation kinetics. Additionally, the presence of  $\delta$ -ferrite in the microstructure is expected to aid the nucleation of bainite because the ferrite–austenite interface is reported in

the literature as a nucleation site for bainitic ferrite.<sup>[19,20]</sup> However, the retarding effect of the higher Mn content of 4.22 wt% (as compared to 2.7–2.9 wt% for the other alloys) was more significant than the other accelerating effects, resulting in a slow transformation time of 4000 s.

Change in length versus time as well as versus temperature curves for the continuous cooling experiments is shown in **Figure 7**. The isothermal transformation times presented in **Figure 6a** were correlated with both the duration of the continuous cooling process, as well as the final microstructures presented in **Figure 8** to ascertain whether the change in length observed is due to bainitic or martensitic transformation.

**Figure 7a–f** illustrates an initial contraction of the dilatometry specimens as the temperature is lowered. This corresponds to the thermal contraction occurring during the brief incubation period before the bainitic transformation begins. **Figure 7c,e** shows an incubation period with a duration of around 100–200 s for all of the conditions studied. **Figure 7a** indicates a transformation that concludes after only a few hundred seconds at a cooling rate of 0.3 K s<sup>-1</sup>. This transformation can only be martensitic because the fastest isothermal bainitic transformation time recorded for a B-group alloy at 350 °C is 2000 s for B3. This is further reinforced by the seemingly fully martensitic microstructure shown in **Figure 7a** for the B1 alloy continuously cooled at 0.3 K s<sup>-1</sup>. Additionally, **Figure 7b** illustrates that for the B1 alloy, the transformation starts at a temperature of 295 °C, which almost coincides with its  $M_s$  of 296 °C. A similar behavior is displayed by the B2 alloy, transforming at 318 °C, which coincides with its  $M_s$ . However, in the case of B2 another transformation is detected at around 250 °C, implying that the bainitic transformation took place below the  $M_s$ . The presence of bainite decorating the prior austenite grain boundaries in B2 continuously cooled at 0.3 K s<sup>-1</sup> was detected under LOM (**Figure 8b**). Bainite formation below the  $M_s$  is well reported in literature.<sup>[19]</sup> A similar behavior to that of B2 is displayed by B3, where an initial transformation starts at 330 °C, which is above a  $M_s$  of 310 °C. This is followed by another transformation at 230 °C, and the microstructure shown in **Figure 8c** also illustrates bainitic ferrite decorating the prior austenite grain boundaries. Conversely, B4 started its transformation at its  $M_s$  of 310 °C, displayed no evidence of a further transformation, and its microstructure (**Figure 8d**) shows the parent austenite transforming to martensite, similar to the behavior of B1.

For the slower cooling rates of 0.03 and 0.003 K s<sup>-1</sup> presented in **Figure 7c–f**, the progress of the bainitic transformation during

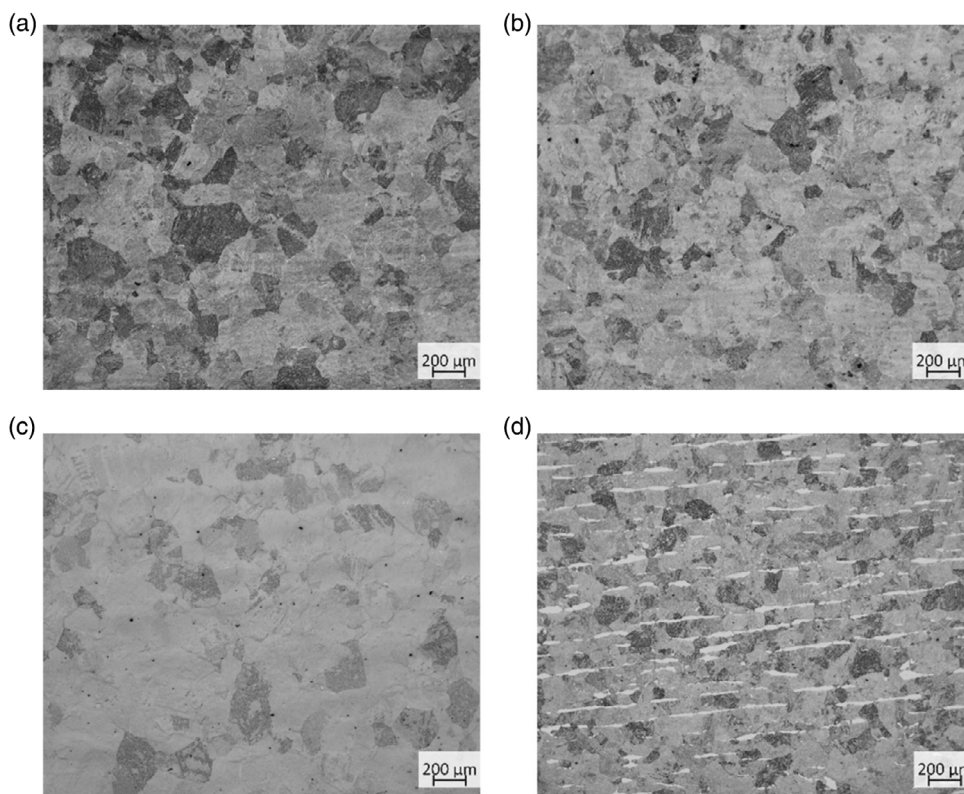


**Figure 5.** LOM images of etched martensitic specimens showing the prior austenite grains in a) B1, b) B2, c) B3, and d) B4.

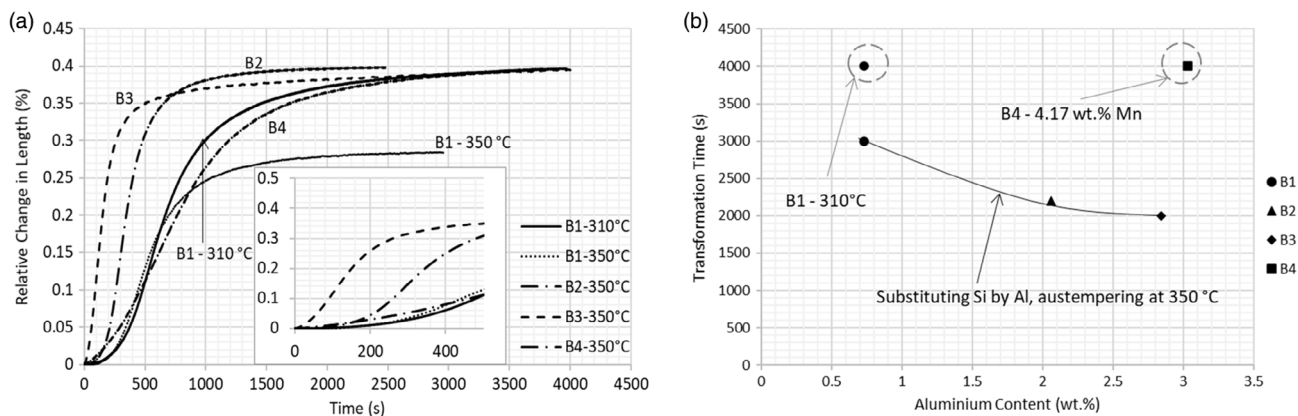


**Figure 6.** a) Dilatometric curves of relative change in length versus time and b) transformation time versus Al content for the isothermally treated conditions.

continuous cooling can be assessed from the progress of the dilatometric change in length versus time curves. A short initial drop in relative change in length represents the short incubation period for the alloys investigated, where the only factor affecting their length change is the thermal contraction brought about by the continuous cooling. This stage is followed by a rapid increase in length that tapers off gradually, representing the bainitic transformation, where the volume expansion associated with  $\gamma$  transforming to bainite is larger than the thermal contraction caused by continuous cooling. Finally, if the bainitic transformation is

concluded, the slope of the relative change in length versus time curve will remain constant; on the other hand, increases in slope (such as the case of B1 continuously cooled from 310 °C at a rate of  $0.03 \text{ K s}^{-1}$ , as shown in Figure 7b) indicate martensite formation.

Lowering the cooling rate to  $0.03$  and  $0.003 \text{ K s}^{-1}$  allowed for sufficient transformation time to conclude the bainitic reaction where, as illustrated in Figure 7c,e, no abrupt increases in relative change in length during the transformation to indicate martensite formation were detected (with the exception of

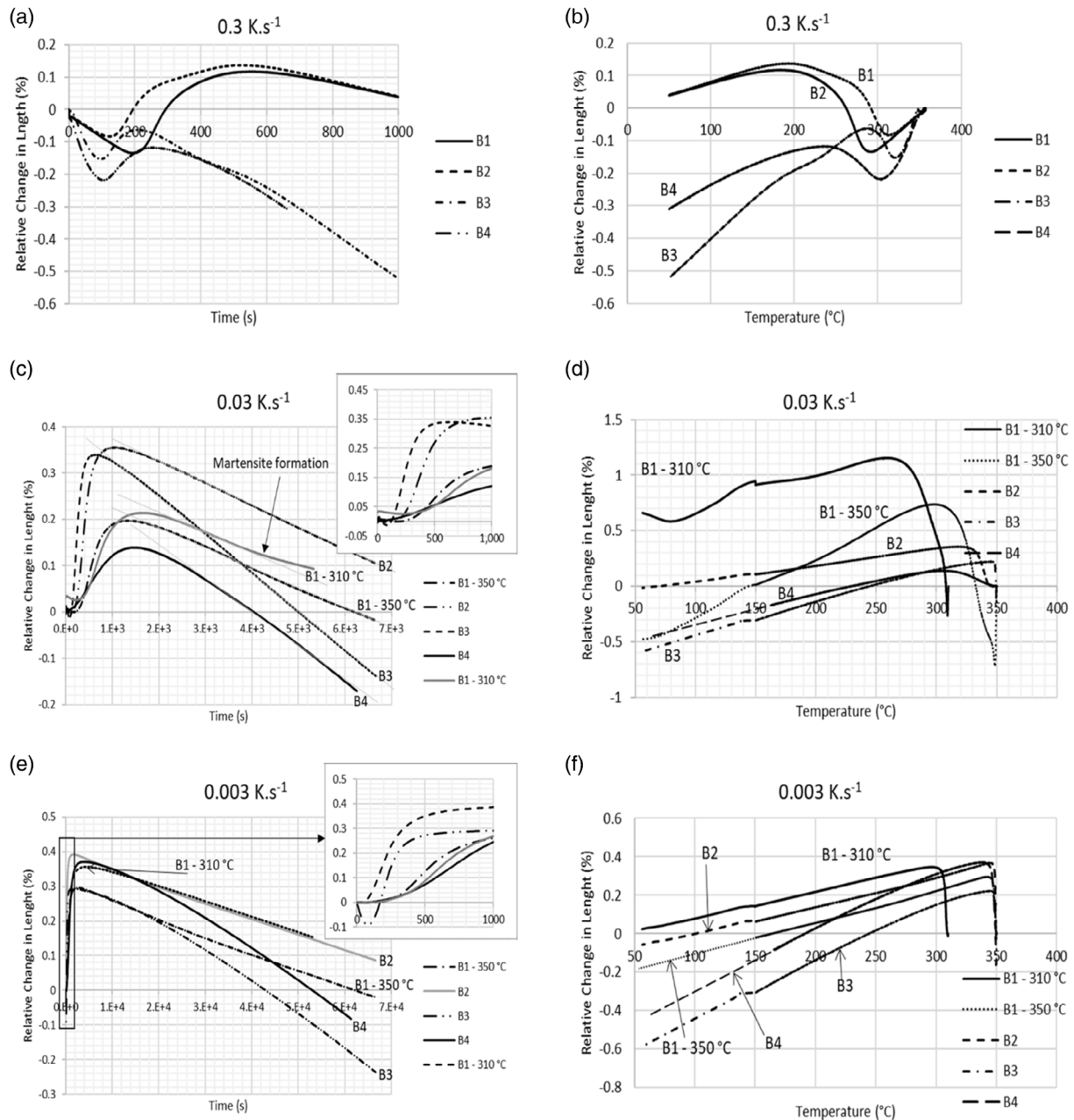


**Figure 7.** a) Relative change in length versus time curves and b) relative change in length versus temperature curves, for specimens continuously cooled at  $0.3 \text{ K s}^{-1}$ . c) Relative change in length versus time curves and d) relative change in length versus temperature curves, for specimens continuously cooled at  $0.03 \text{ K s}^{-1}$ . e) Relative change in length versus time curves and f) relative change in length versus temperature curves, for specimens continuously cooled at  $0.003 \text{ K s}^{-1}$ .

the aforementioned B1, cooled from  $310 \text{ }^\circ\text{C}$  at a rate of  $0.03 \text{ K s}^{-1}$ . It is evident from Figure 7c,e that the maximum transformation rate (peak of the length change curve) occurs after Final less than 2000 s, corresponding to a temperature  $300\text{--}325 \text{ }^\circ\text{C}$  at a cooling rate of  $0.03 \text{ K s}^{-1}$  (Figure 7d), and a temperature of around  $340 \text{ }^\circ\text{C}$  at a rate of  $0.003 \text{ K s}^{-1}$  (Figure 7f). The presented results imply that at both rates of 0.03 and  $0.003 \text{ K s}^{-1}$ , most of the transformation could be concluded above the initial  $M_s$ . Additionally, as more bainitic ferrite is formed,

excess carbon is rejected to the remaining austenite enriching it, lowering the  $M_s$  further and enabling the conclusion of the reaction as the temperature is dropped during continuous cooling.

### 3.3. Developed Microstructure

Figure 9a–d shows SEM micrographs of the alloys with the typical morphology of a nB microstructure of bainitic ferrite lamellae

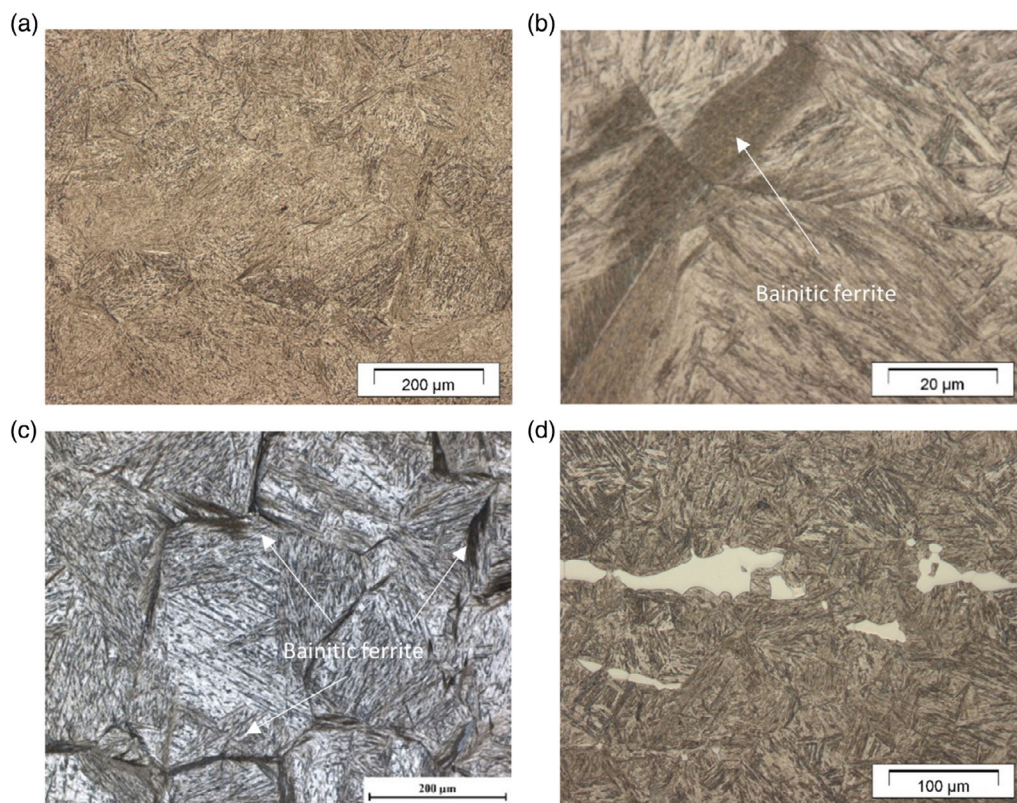


**Figure 8.** Micrographs of a) the B1 alloy continuously cooled at  $0.3 \text{ K s}^{-1}$  showing a fully martensitic microstructure; b) the B2 alloy and c) the B3 alloy, continuously cooled at  $0.3 \text{ K s}^{-1}$  showing a martensitic microstructure with bainitic ferrite decorating the prior austenite grain boundaries; and d) the B1 alloy continuously cooled at  $0.3 \text{ K s}^{-1}$  showing a fully martensitic transformation.

and islands of  $\gamma_r$  interspersed in the microstructure. Additionally, the presence of large martensite grains was detected for some conditions; the observable difference in size between the stable blocky austenite in Figure 9a and the larger austenite grain that transformed to martensite in Figure 9b is in agreement with the literature reports of the effect of austenite size on its stability during cooling.<sup>[21]</sup> Figure 9c shows the microstructure of a continuously cooled B3 specimen; the bainitic lamellae in the microstructure display different thicknesses as the incremental reduction of temperature throughout the process causes finer bainite to form as the transformation progresses. TEM investigations were performed on selected conditions and given in Figure 9e–h, showing that the interlath as well as the intralath cementite particles are absent. This indicates the effectiveness of substituting Si by Al in suppressing the cementite formation and hence obtaining carbide free bainite structures. The TEM micrographs also revealed the high dislocation density in the bainitic ferrite laths, developed during bainite formation.

### 3.4. Retained Austenite Analysis

X-ray diffraction (XRD) patterns for the isothermally treated conditions are shown in Figure 10a. The continuously cooled conditions were not presented in Figure 10 as they cannot be associated with a single transformation temperature on the  $T_0$  curve; however, the  $\gamma_r$  volume fraction results for the

continuously cooled conditions are presented in the following section. The  $\gamma_r$  volume fraction and its lattice parameter  $a_{\gamma_r}$  were calculated from the obtained XRD patterns.<sup>[16]</sup> The C content of the  $\gamma_r$  ( $C_{\gamma_r}$ ) was calculated from its  $a_{\gamma_r}$  using the Dyson and Holmes Equation (1)<sup>[22]</sup>

$$C_{\gamma} = (a_{\gamma} - 0.3578 - 0.000095w_{\text{Mn}} - 0.00056w_{\text{Al}} - 0.00031w_{\text{Mo}}) / 0.0033 \quad (1)$$

The  $C_{\gamma}$  results obtained from Equation (1) were plotted alongside the theoretical  $T_0$  curves simulated using ThermoCalc TCFE9 database and the results are provided in Figure 8b. ThermoCalc simulations show that increasing the Al content from 0.7 wt% in B1 to 2.8 wt% in B3 shifts the  $T_0$  curve to the left contrary to the established literature, which associates an increase in Al content with a shift in the  $T_0$  curve toward higher C contents.<sup>[23]</sup> On the other hand, experimentally obtained  $C_{\gamma}$  values for the B2, B3, and B4 alloys lie in good agreement with the simulated  $T_0$  curves, albeit with slightly lower  $C_{\gamma}$  amounts. It should be noted that the solute partitioning in B4 is not expected to affect the  $T_0$  results because, as discussed in Section 3.1, the changes in Al and Mn contents are marginal, and variations in C content have been reported in the literature to have an insignificant effect on the  $T_0$  curves.<sup>[24]</sup> Experimentally obtained  $C_{\gamma}$  values commonly exceed those obtained from  $T_0$  curves, owing to the measurements being skewed toward the



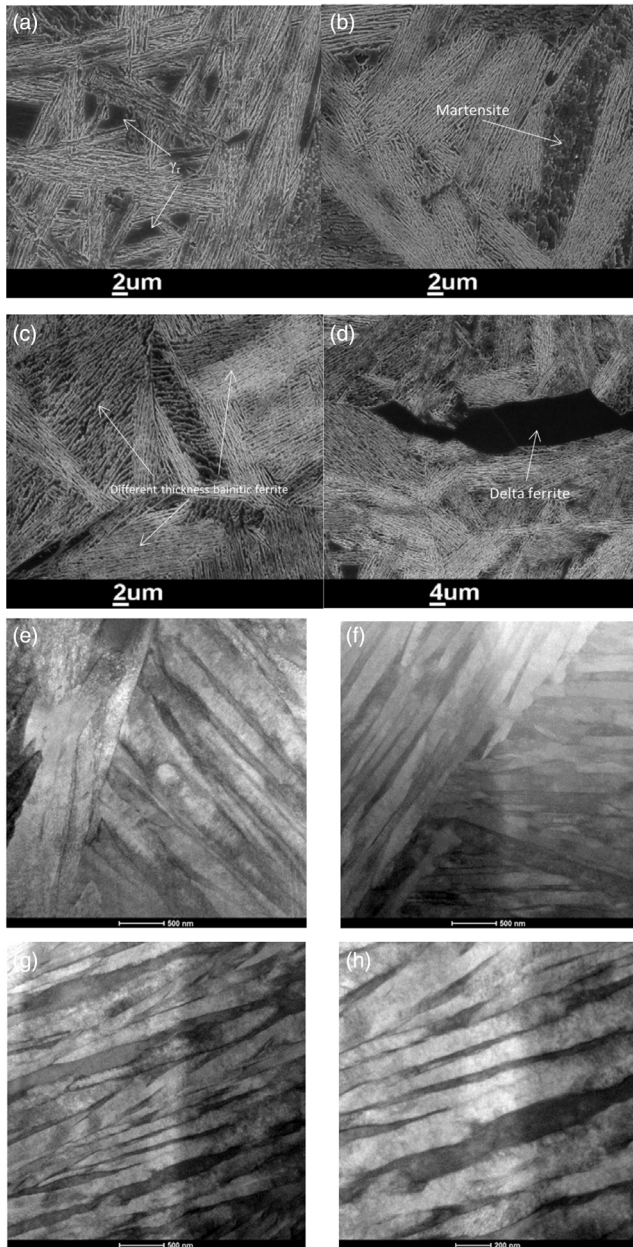


**Figure 9.** SEM micrographs for a) B1 isothermally treated at 350 °C, b) B2 isothermally treated at 350 °C, c) B3 continuously cooled at 0.03 K s<sup>-1</sup>, d) B4 isothermally treated at 350 °C, and TEM micrographs of e) B1 isothermally treated at 350 °C, f) B2 isothermally treated at 350 °C, and g,h) B3 isothermally treated at 350 °C.

more supersaturated (hence more stable)  $\gamma$ -film as a result of a fraction of the blocky  $\gamma$  transforming to martensite during cooling.<sup>[25]</sup> However, this was only observed in the case of B1, where the experimental  $C_\gamma$  values were much higher than those predicted by ThermoCalc. These observations imply a higher amount of unstable austenite in the B1 alloy, which, in turn, indicates that the addition of Al helped improve the stability of the retained austenite in B2, B3, and B4 alloys. While Al is a ferrite stabilizer expected to lower the stability of austenite by being in

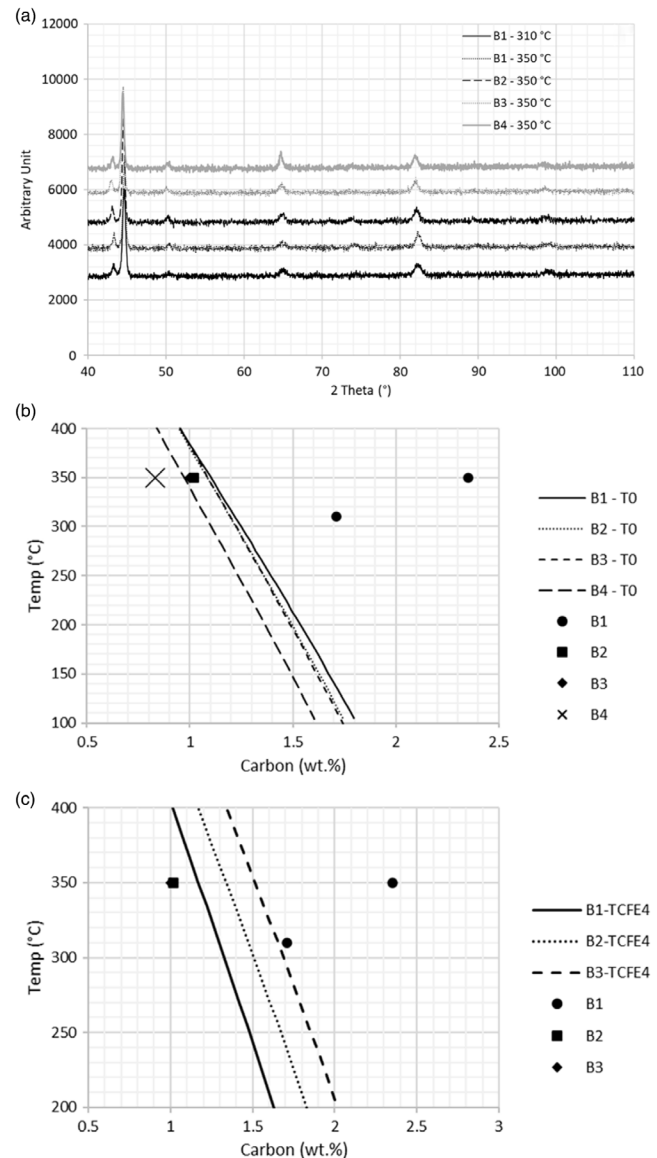


**Figure 10.** a) XRD patterns for the alloys B1 through B4 in the isothermally treated condition, b)  $T_0$  curves simulated via ThermoCalc plotted with the  $C_\gamma$  values experimentally obtained from Equation (1) for the isothermally treated conditions, and c)  $T_0$  curves simulated via the TCFE4 database plotted with the  $C_\gamma$  values experimentally obtained from Equation (1) for the isothermally treated conditions.

the solid solution, it is expected to improve the stability of retained austenite in a nB microstructure by increasing the driving force for bainite transformation, leading to more bainitic ferrite forming and consequently enriching the retained austenite with C. This enriched retained austenite is less likely to transform into martensite upon cooling and will yield  $C_\gamma$  results similar to those of B2 through B4. This analysis is further supported by the retained austenite measurements provided in a later section. Additionally, it should be noted that the  $T_0$  curve for B4 recorded the lowest carbon amounts owing to the higher amount of Mn present in the alloy.

The alloys B1–B3 represent a constant chemical composition with only a change in Al (and Si; however, ThermoCalc predictions indicate that Si would have no significant effect on the  $T_0$  curve), therefore would be ideal for gaining insights on how different ThermoCalc databases calculate the effect of Al on the  $T_0$  curve of an alloy. Theoretical  $T_0$  curves simulated using the older TCFE4 database (with which the original alloy design was performed during the early research proposal writing phase) and presented in Figure 10c are in line with the trends in the aforementioned literature, with the  $T_0$  C content increasing as the Al content is increased from B1 to B3. However, the TCFE4 database associates higher C contents with the  $T_0$  curves of the alloys investigated than those calculated using the TCFE9 shifting the values further away from those experimentally obtained. While the TCFE4 database presents predictions that are in line with the current understanding of the effect of Al on the  $T_0$  curve, as shown from the results in Figure 10b,c this understanding does not reflect the experimentally obtained  $C_\gamma$  values, and while the TCFE9 falls short in predicting the A3 temperature and the  $T_0$  curve for B1, it presents an adequate prediction for the effect of Al on the  $T_0$  curve.

### 3.5. Mechanical Behavior

Figure 11 shows the stress–strain curves for (a) the isothermally treated conditions, (b) and (c) the conditions continuously cooled at 0.03 and 0.003 K s<sup>-1</sup>, respectively, and (d) a comparison between isothermal treatment and continuous cooling for B1 and B2, as well as the tensile strength versus total elongation (EL%) for (e) the isothermally treated conditions and (f) the continuously cooled ones. Figure 11a,e reveals that as the Al content is increased from 0.73 to 2.8 wt% (alloys B1 to B3), a small reduction in tensile strength from 1330 to 1270 MPa was observed. The highest value of 1520 MPa could be recorded for alloy B1 austempered at 310 °C, which was enabled by its lower  $M_s$ , resulting in finer bainitic lamellae. On the other hand, the cost of such a high tensile strength was an extended transformation time of 4000 s, as shown in Figure 6. In terms of ductility, EL drops from 13.5% to 7.7% as the Al content is increased from 0.73 to 2.8 wt%. Alloy B4, containing ≈12 vol%  $\delta$ -ferrite, recorded the lowest tensile strength with only 1105 MPa; however, its ductility was the highest with 16% among the conditions tested. As illustrated in Figure 11e, a significant loss of the strength–ductility balance is accompanying the replacement of Si by Al with a drop from 13.5% (B1) to 7.7% (B3) for the conditions isothermally treated at 350 °C. A similar trend emerged for the continuously cooled specimens (Figure 11f) with EL dropping from 10% (B1) to 8.4% (B3) for the conditions quenched to 350 °C (CC350) followed by continuous cooling at a rate of 0.03 K s<sup>-1</sup> and from 12.8% (B1) to 9.9 and 10.4% (B2 and B3, respectively) for the cooling rate of 0.003 K s<sup>-1</sup>.

Improved tensile properties were obtained via continuous cooling. Figure 11d,f shows a tensile strength increase of approximately 100 MPa for the isothermally treated conditions after continuously cooling at a rate of 0.03 K s<sup>-1</sup>. On the other hand, continuous cooling at 0.003 K s<sup>-1</sup> provides no significant change in strength compared to the isothermal treatment, with its stress

strain curves almost coinciding with those obtained after isothermal treatment (Figure 11d). The constant decrease in transformation temperature during continuous cooling is expected to refine the bainitic lamellar thickness. This benefits from a continued reduction in  $M_s$  the more the transformation progresses as a result of austenite enrichment with carbon. However, the previous statement is only valid provided that the  $M_s$  temperature is not reached before the bainitic reaction is concluded. This lamellar refinement was evident in the tensile test results of the conditions cooled at a rate of 0.03 K s<sup>-1</sup>, which recorded values approximately 100 MPa higher than the isothermally treated conditions. On the other hand, the slow cooling rate of 0.003 K s<sup>-1</sup> allowed sufficient time for the transformation to conclude near the starting temperature, with the drop in temperature from 350 to 340 °C requiring approximately 3300 s, which is comparable to the time required for the slowest transforming alloys to finish the bainitic reaction in the isothermal condition. Therefore, no difference in results was noticed when compared to the isothermally treated condition.

Conversely, no difference in the elongation values was observed between the isothermally treated and the continuously cooled conditions, with the overall average of all the conditions for the alloys B1–B3 being approximately 10%. Alloy B4 also recorded the highest EL with 15% owing to its 12 vol%  $\delta$ -ferrite. On the other hand, the B1 specimens quenched to 310 °C and continuously cooled with 0.03 K s<sup>-1</sup> recorded a low EL of 7.1%. Figure 12a shows the relative change in length versus time for a B1 specimen quenched to 310 °C and continuously cooled with 0.03 K s<sup>-1</sup>. An increase in length toward the end of the transformation indicates martensite formation, formed after approximately 4000 s of transformation and at a corresponding temperature of approximately 190 °C. SEM images of the specimens (Figure 12b) confirm the presence of large regions of martensite in the microstructure, explaining the significantly higher strength as well as lower ductility for this condition. The current results indicate that for nB alloys with a transformation time of around an hour, a continuous cooling rate in the order of 10<sup>-2</sup> is the most suitable to refine the microstructure. Hardness testing results presented in Figure 12c indicate a tendency for the hardness of the conditions continuously cooled at 0.03 K s<sup>-1</sup> to record a higher HV30 value than the isothermal condition for the lower Al B1 and B2 alloys, implying a higher content of martensite in the final microstructure. However, upon lowering the cooling rate to 0.003 K s<sup>-1</sup>, the hardness values drop to levels similar to those obtained via isothermal holding. Conversely, this trend is absent in the higher Al-content alloy B3, which recorded similar hardness values for all of the conditions tested owing to its much faster transformation kinetics.

Plotting the impact energy values versus the alloy's Al content (Figure 13a,b) reveals that, for both the isothermally treated and continuously cooled conditions, the impact properties increase as the Al content increases from 0.7 to 2 wt%. This is followed by a drop with the further increase of Al to 2.8 wt% while remaining higher than the original value. The lowest impact properties, however, were recorded for B4, owing to the presence of  $\delta$ -ferrite. The large, elongated morphology of  $\delta$ -ferrite (Figure 9d) as well as the segregation of Mn atoms along their boundaries is reported in the literature to provide weakened paths for crack

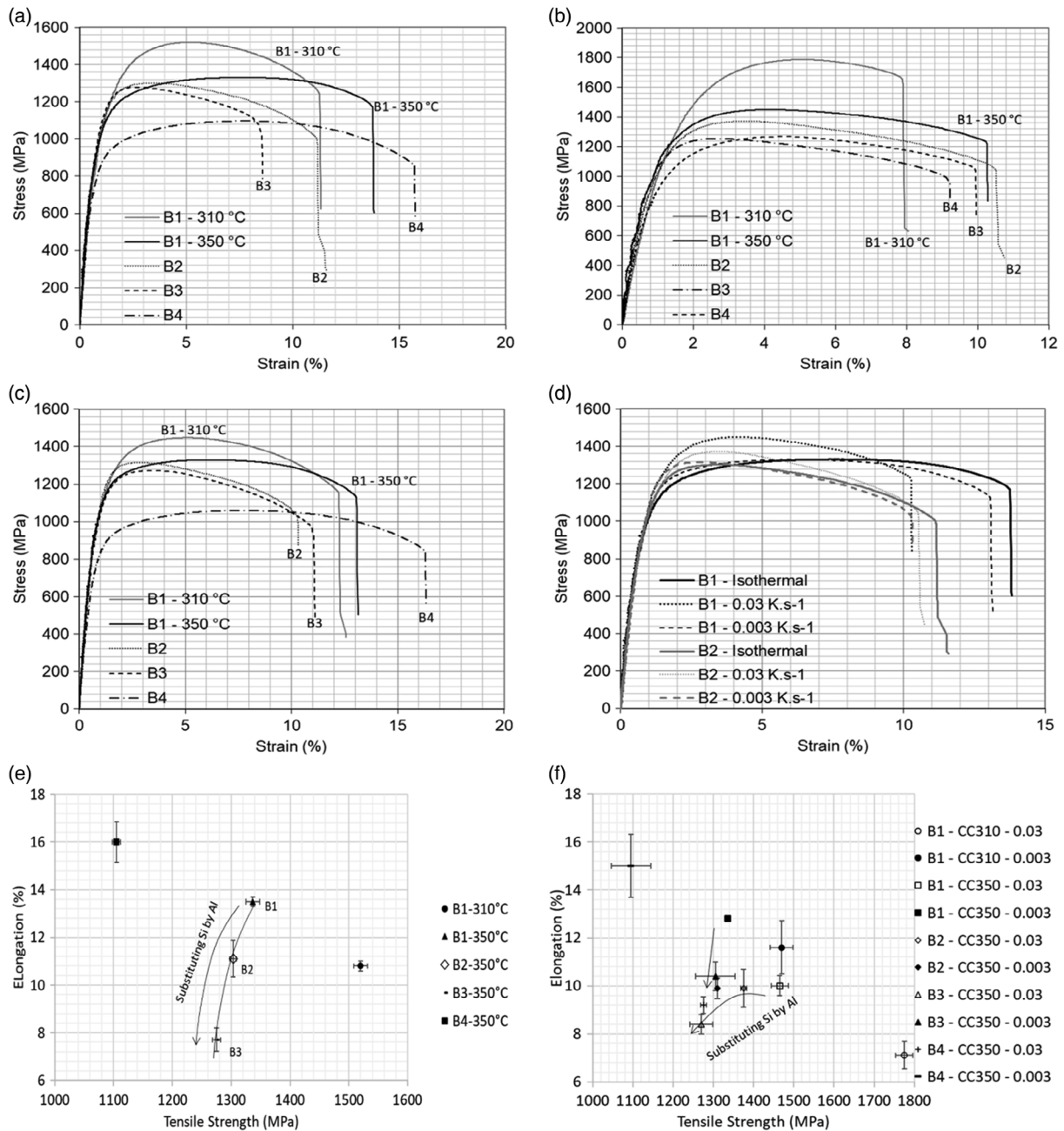


**Figure 11.** Stress–strain curves for a) isothermally treated conditions, continuously cooled at a rate of b)  $0.03 \text{ K s}^{-1}$ , c)  $0.003 \text{ K s}^{-1}$ , d) comparison between the stress–strain curves of B1 and B2 in isothermal and continuously cooled conditions, and e) the isothermally treated conditions, and f) continuously cooled conditions.

propagation in  $\delta$ -ferrite-containing microstructures, deteriorating their overall impact properties.<sup>[26]</sup>

Two main factors govern the mechanical properties of nB microstructures: the lamellar thickness controls the strength, while the amount of  $\gamma_r$  controls the ductility. The bainitic lamellar thickness plotted versus Al content presented in **Figure 14a** illustrates that as the Al content increases from 0.7 to 2.0 and 2.8 wt% (B1, B2, and B3, respectively), a drop in lamellar thickness of approximately 15 nm is observed. However, the tensile

strength values plotted against bainitic thickness (Figure 14b) only vary slightly between the different conditions, remaining at a level of 1300 MPa. The simulated  $T_0$  curves presented in Figure 10b indicate that the highest bainite fraction (and consequently lowest  $\gamma_r$  one) is expected for the B1 alloy. Additionally, as previously mentioned, Figure 10b also implies a lower stability for  $\gamma_r$  in B1 than the other alloys and, consequently, higher martensite fraction in that alloy. Both the aforementioned factors are consistent with both the tensile strength

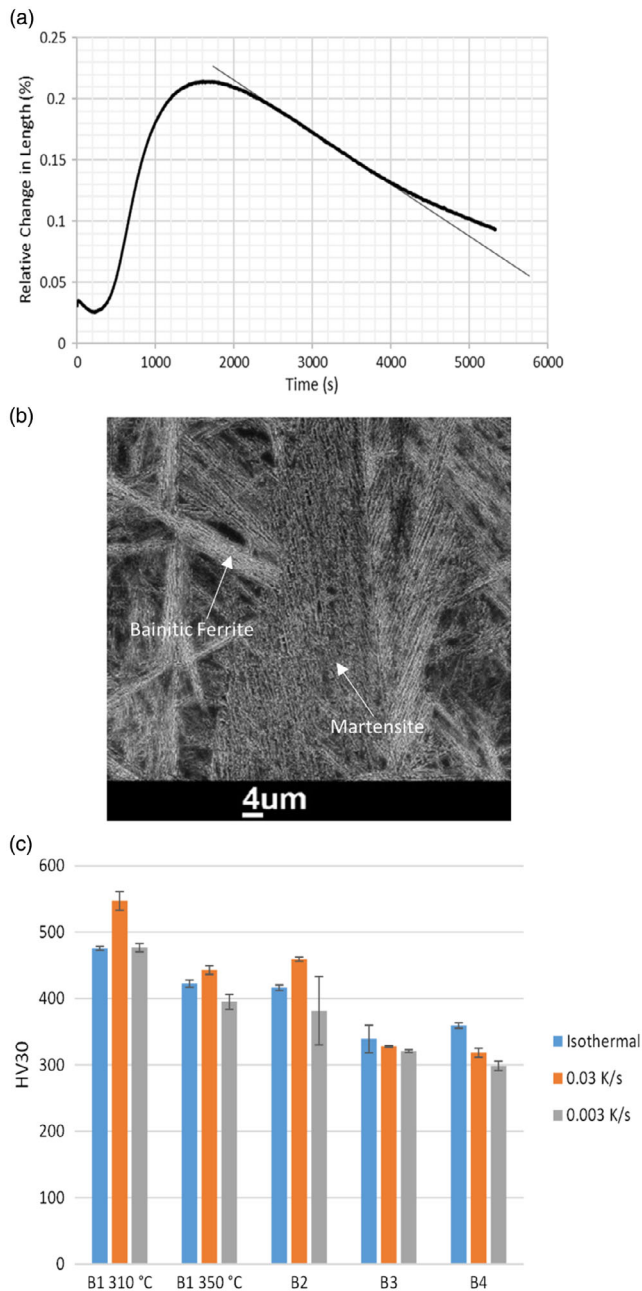


**Figure 12.** a) Relative change in length versus time for the B1 alloy quenched to 310 °C and continuously cooled at 0.03 K s<sup>-1</sup>; b) SEM image of the aforementioned condition.

results and the  $\gamma_r$  % results presented in Figure 14b,c, respectively. The decrease in bainite content with increasing Al addition is due to a lower amount of martensite in the higher Al conditions as previously discussed in Section 3.4. The XRD would include martensite as part of its ferrite measurement, which is the reason why B1 has the lowest  $\gamma_r$  values and the highest strength even though it recorded the highest lamellar thickness among the alloys studied. Conversely, as the Al content increases in B2 through B4, the amount of retained austenite slightly increases (Figure 14c), which is related to a higher

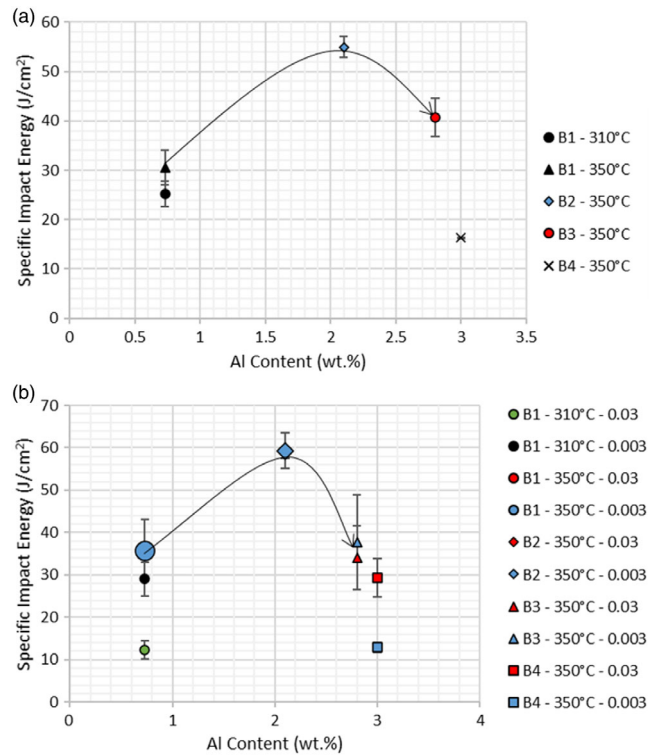


**Figure 13.** Specific impact energy versus Al content (wt%) for the a) isothermally treated and b) continuously cooled conditions.

stability of the retained austenite at room temperature rather than a lower amount of bainitic ferrite. Additionally, effect of the increased Al in refining the lamellar thickness for B2 and B3 resulted in their tensile strengths being comparable to B1 which has higher martensite in its microstructure. On the other hand, no visible trends could be discerned from plotting the amount of  $\gamma_r$  versus EL. However, this is possible as neither microscopy nor XRD analysis can accurately quantify the amount of martensite in the conditions investigated, which is expected to have a significant influence on the ductility of the microstructures in question.

## 4. Conclusions

A low-cost strategy for producing LC nB microstructures was developed using addition of Al to accelerate the bainite transformation. Increasing the Al content from 0.7 to 2.8 wt% in alloys B1–B3 resulted in a drop in transformation times from 3000 to 2000 s. The B4 alloy with 12 vol%  $\delta$ -ferrite recorded a slower transformation time of 4000 s despite its lower C of 0.23 wt% and higher Al of 3 wt%; this was attributed to its higher Mn content of 4.17 wt% added to maintain an acceptably low  $M_s$ . Conversely, accelerating the transformation via Al addition came at a cost of a slight drop in Tensile strengths from 1370 to 1270 MPa and a reduction in EL% from 13.5% to 7.7%. Additionally, the specific impact energy increased from 30 to 55 J cm<sup>-2</sup> as the Al content increased from 0.7 to 2 wt %, followed by a further drop to 40 J cm<sup>-2</sup> for the B3 alloy with

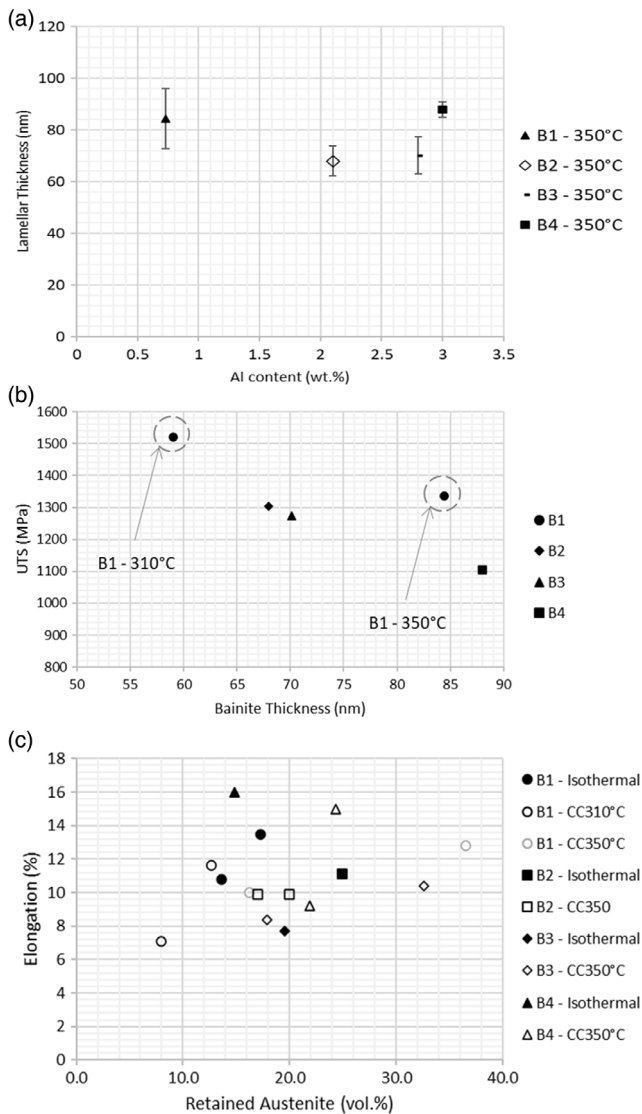


**Figure 14.** a) UTS versus bainitic lamellar thickness, b) EL (%) versus amount of  $\gamma_r$  (vol%), c) bainitic lamellar thickness versus Al content.

2.8 wt% Al. While the highest EL% value was recorded at 16% for the B4 alloy with 12 vol%  $\delta$ -ferrite, this came at a cost of a lower tensile strength of 1105 MPa. Additionally, the presence of  $\delta$ -ferrite caused a deterioration in the impact properties, lowering it to a value of  $16.3 \text{ J cm}^{-2}$ . Continuously cooling at a rate of  $0.03 \text{ K s}^{-1}$  yielded improved tensile strength at the same EL, while a rate of  $0.3 \text{ K s}^{-1}$  resulted in martensite formation, and a much slower rate of  $0.003 \text{ K s}^{-1}$  did not yield different properties from the isothermally treated conditions. When replacing Si with Al, a significant loss of the strength–ductility balance is observed in both the isothermally treated as well as the continuously cooled conditions, with an optimum compromise between transformation time and mechanical properties found in the B2 alloy with 2 wt% Al. Finally, discrepancies between

thermodynamic simulation results obtained via ThermoCalc and the experimental trends imply that the thermodynamics effects of Al on the of the transformation behavior in steels need further investigations to be finally implemented into the simulation source.

## Acknowledgements

This work was funded by the German Research Foundation (DFG), grant number: DFG SO 1250/1.

Open access funding enabled and organized by Projekt DEAL.

## Conflict of Interest

The authors declare no conflict of interest.

## Data Availability Statement

The raw/processed data required to reproduce these findings cannot be shared at this time as the data also forms part of an ongoing study.

## Keywords

Al content, low carbon, mechanical properties, nanobainite

Received: September 10, 2021

Revised: December 9, 2021

Published online: December 29, 2021

- [1] H.-S. Yang, H. K. D. H. Bhadeshia, *Mater. Sci. Technol.* **2008**, 24, 335.
- [2] S. Das, A. Haldar, *Metall. Mater. Trans A* **2014**, 45, 1844.
- [3] C. Garcia-Mateo, G. Paul, M. Somani, D. Porter, L. Bracke, A. Latz, C. Garcia De Andres, F. Caballero, *Metals* **2017**, 7, 159.
- [4] F. G. Caballero, C. Garcia-Mateo, *Encycl. Mater., Metals Alloy* **2020**, 69, 73.
- [5] M. Foughani, A. Kolahi, Y. Palizdar, *AIP Conf. Proc.* **2018**, 20024.
- [6] M. Soliman, H. Mostafa, A. S. El-Sabbagh, H. Palkowski, *Mater. Sci. Eng., A* **2010**, 527, 7706.
- [7] H. Mousalou, S. Yazdani, B. Avishan, N. P. Ahmadi, A. Chabok, Y. Pei, *Mater. Sci. Eng., A* **2018**, 734, 329.
- [8] S. P. Neog, S. D. Bakshi, S. Das, *Wear* **2020**, 456–457, 203359.
- [9] S. M. Hasan, M. Ghosh, D. Chakrabarti, S. B. Singh, *Mater. Sci. Eng., A* **2020**, 771, 138590.
- [10] M. Soliman, H. Palkowski, *Arch. Civ. Mech. Eng.* **2016**, 16, 403.
- [11] J. Yang, H. Qiu, P. Xu, H. Yu, Y. Wang, *AIP Conf. Proc.* **2018**, 20001.
- [12] a) J. Kang, Y. J. Li, X. H. Wang, H. S. Wang, G. Yuan, R. D. K. Misra, G. D. Wang, *Mater. Sci. Eng., A* **2019**, 742, 464; b) F. G. Caballero, H. K. D. H. Bhadeshia, *Curr. Opin. Solid State Mater. Sci.* **2004**, 8, 251.
- [13] M. Soliman, B. Weidenfeller, H. Palkowski, *Steel Res. Int.* **2009**, 80, 57.
- [14] M. Soliman, H. Palkowski, *Mater. Des.* **2015**, 88, 759.
- [15] L. B. S. Bechet, *Rev. Metall.* **1955**, 52, 830.
- [16] B. D. Cullity, S. R. Stock, *Elements of X-Ray Diffraction*, Pearson/Prentice Hall, Upper Saddle River, NJ **2001**.
- [17] M. Akram, M. Soliman, H. Palkowski, *Metals* **2021**, 11, 1210.

- [18] C. Garcia-Mateo, F. G. Caballero, H. K. D. H. Bhadeshia, *ISIJ Int.* **2003**, *43*, 1821.
- [19] W. Gong, Y. Tomota, S. Harjo, Y. H. Su, K. Aizawa, *Acta Mater.* **2015**, *85*, 243.
- [20] H. K. D. H. Bhadeshia, J. W. Christian, *Metall. Mater. Trans A* **1990**, *21*, 767.
- [21] S. Lee, S.-J. Lee, B. C. de Cooman, *Scr. Mater.* **2011**, *65*, 225.
- [22] D. J. Dyson, B. Holmes, *J. Iron Steel Inst* **1970**, *208*, 469.
- [23] H. I. Aaronson, H. A. Domian, G. M. Pound, *Trans. Metall. Soc. AIME* **1967**, *236*, 768.
- [24] M. Soliman, H. Palkowski, *ISIJ Int.* **2007**, *47*, 1703.
- [25] H. K. D. H. Bhadeshia, D. V. Edmonds, *Mater. Sci.* **1983**, *17*, 420.
- [26] M. T. Kim, T. M. Park, K.-H. Baik, W. S. Choi, P.-P. Choi, J. Han, *Acta Mater.* **2019**, *164*, 122.